

# Energy dependence of particle ratio fluctuations in central Pb+Pb collisions from $\sqrt{s_{NN}} = 6.3$ to 17.3 GeV

C. Alt,<sup>9</sup> T. Anticic,<sup>21</sup> B. Baatar,<sup>8</sup> D. Barna,<sup>4</sup> J. Bartke,<sup>6</sup> L. Betev,<sup>10</sup> H. Białkowska,<sup>19</sup> C. Blume,<sup>9</sup> B. Boimska,<sup>19</sup> M. Botje,<sup>1</sup> J. Bracinik,<sup>3</sup> R. Bramm,<sup>9</sup> P. Bunčić,<sup>10</sup> V. Cerny,<sup>3</sup> P. Christakoglou,<sup>2</sup> O. Chvala,<sup>14</sup> J.G. Cramer,<sup>16</sup> P. Csató,<sup>4</sup> P. Dinkelaker,<sup>9</sup> V. Eckardt,<sup>13</sup> D. Flierl,<sup>9</sup> Z. Fodor,<sup>4</sup> P. Foka,<sup>7</sup> V. Friese,<sup>7</sup> J. Gál,<sup>4</sup> M. Gaździcki,<sup>9,11</sup> V. Genchev,<sup>18</sup> G. Georgopoulos,<sup>2</sup> E. Gładysz,<sup>6</sup> K. Grebieszko,<sup>20</sup> S. Hegyi,<sup>4</sup> C. Höhne,<sup>7</sup> K. Kadija,<sup>21</sup> A. Karev,<sup>13</sup> M. Kliemant,<sup>9</sup> S. Kniege,<sup>9</sup> V.I. Kolesnikov,<sup>8</sup> E. Kornas,<sup>6</sup> R. Korus,<sup>11</sup> M. Kowalski,<sup>6</sup> I. Kraus,<sup>7</sup> M. Kreps,<sup>3</sup> D. Kresan,<sup>7</sup> M. van Leeuwen,<sup>1</sup> P. Lévai,<sup>4</sup> L. Litov,<sup>17</sup> B. Lungwitz,<sup>9</sup> M. Makariev,<sup>17</sup> A.I. Malakhov,<sup>8</sup> M. Mateev,<sup>17</sup> G.L. Melkumov,<sup>8</sup> A. Mischke,<sup>1</sup> M. Mitrovski,<sup>9</sup> J. Molnár,<sup>4</sup> St. Mrówczyński,<sup>11</sup> V. Nicolich,<sup>21</sup> G. Pálfa,<sup>4</sup> A.D. Panagiotou,<sup>2</sup> D. Panayotov,<sup>17</sup> A. Petridis<sup>†,2</sup> M. Pikna,<sup>3</sup> D. Prindle,<sup>16</sup> F. Pühlhofer,<sup>12</sup> R. Renfordt,<sup>9</sup> C. Roland,<sup>5</sup> G. Roland,<sup>5</sup> M. Rybczyński,<sup>11</sup> A. Rybicki,<sup>22</sup> A. Sandoval,<sup>7</sup> N. Schmitz,<sup>13</sup> T. Schuster,<sup>9</sup> P. Seyboth,<sup>13</sup> F. Siklér,<sup>4</sup> B. Sitar,<sup>3</sup> E. Skrzypczak,<sup>20</sup> G. Stefanek,<sup>11</sup> R. Stock,<sup>9</sup> H. Ströbele,<sup>9</sup> T. Susa,<sup>21</sup> I. Szentpétery,<sup>4</sup> J. Sziklai,<sup>4</sup> P. Szymanski,<sup>10,19</sup> V. Trubnikov,<sup>19</sup> D. Varga,<sup>4,10</sup> M. Vassiliou,<sup>2</sup> G.I. Veres,<sup>4,5</sup> G. Vesztergombi,<sup>4</sup> D. Vranić,<sup>7</sup> A. Wetzler,<sup>9</sup> Z. Włodarczyk,<sup>11</sup> I.K. Yoo,<sup>15</sup> and J. Zimányi<sup>†,4</sup>

(The NA49 collaboration)

<sup>1</sup>NIKHEF, Amsterdam, Netherlands.

<sup>2</sup>Department of Physics, University of Athens, Athens, Greece.

<sup>3</sup>Comenius University, Bratislava, Slovakia.

<sup>4</sup>KFKI Research Institute for Particle and Nuclear Physics, Budapest, Hungary.

<sup>5</sup>MIT, Cambridge, USA.

<sup>6</sup>Institute of Nuclear Physics, Cracow, Poland.

<sup>7</sup>Gesellschaft für Schwerionenforschung (GSI), Darmstadt, Germany.

<sup>8</sup>Joint Institute for Nuclear Research, Dubna, Russia.

<sup>9</sup>Fachbereich Physik der Universität, Frankfurt, Germany.

<sup>10</sup>CERN, Geneva, Switzerland.

<sup>11</sup>Institute of Physics Świątokrzyska Academy, Kielce, Poland.

<sup>12</sup>Fachbereich Physik der Universität, Marburg, Germany.

<sup>13</sup>Max-Planck-Institut für Physik, Munich, Germany.

<sup>14</sup>Institute of Particle and Nuclear Physics, Charles University, Prague, Czech Republic.

<sup>15</sup>Department of Physics, Pusan National University, Pusan, Republic of Korea.

<sup>16</sup>Nuclear Physics Laboratory, University of Washington, Seattle, WA, USA.

<sup>17</sup>Atomic Physics Department, Sofia University St. Kliment Ohridski, Sofia, Bulgaria.

<sup>18</sup>Institute for Nuclear Research and Nuclear Energy, Sofia, Bulgaria.

<sup>19</sup>Institute for Nuclear Studies, Warsaw, Poland.

<sup>20</sup>Institute for Experimental Physics, University of Warsaw, Warsaw, Poland.

<sup>21</sup>Rudjer Boskovic Institute, Zagreb, Croatia.

<sup>22</sup>Henryk Niewodniczanski Institute of Nuclear Physics, Polish Academy of Sciences, Cracow, Poland.

<sup>†</sup>deceased

(Dated: August 17, 2021)

We present recent measurements of the energy dependence of event-by-event fluctuations in the  $K/\pi$  and  $(p + \bar{p})/\pi$  multiplicity ratios in heavy ion collisions at the CERN SPS. The particle ratio fluctuations were obtained for central Pb+Pb collisions at five collision energies,  $\sqrt{s_{NN}}$ , between 6.3 and 17.3 GeV. After accounting for the effects of finite-number statistics and detector resolution, we extract the strength of non-statistical fluctuations at each energy. For the  $K/\pi$  ratio, larger fluctuations than expected for independent particle production are found at all collision energies. The fluctuations in the  $(p + \bar{p})/\pi$  ratio are smaller than expectations from independent particle production, indicating correlated pion and proton production from resonance decays. For both ratios, the deviation from purely statistical fluctuations shows an increase towards lower collision energies. The results are compared to transport model calculations, which fail to describe the energy dependence of the  $K/\pi$  ratio fluctuations.

## I. INTRODUCTION

Quantum Chromodynamics predicts that at sufficiently high temperature, strongly interacting matter will undergo a phase transition from hadronic matter to a state characterized by quark and gluon degrees of free-

dom, the quark-gluon plasma (QGP) [1]. Experimentally, strongly interacting matter under extreme conditions can be created in heavy ion collisions at highly relativistic energies. Experiments have been performed over a very large range of center of mass collision energies,  $\sqrt{s_{NN}}$ , including  $2.3 \text{ GeV} < \sqrt{s_{NN}} < 4.9 \text{ GeV}$  at the

Brookhaven Alternating Gradient Synchrotron (AGS),  $6.3 \text{ GeV} < \sqrt{s_{NN}} < 17.3 \text{ GeV}$  at the CERN Super Proton Synchrotron (SPS) and  $19.6 \text{ GeV} < \sqrt{s_{NN}} < 200 \text{ GeV}$  at the Brookhaven Relativistic Heavy Ion Collider (RHIC).

In the SPS energy range, several hadronic observables in central Pb+Pb collisions show qualitative changes in their energy dependence. The ratio of average  $\langle K^+ \rangle$  to  $\langle \pi^+ \rangle$  yields exhibits non-monotonic behavior in the low-energy SPS range, close to  $\sqrt{s_{NN}} \approx 7.6 \text{ GeV}$  [2]. In the same energy range, the slopes of the hadron transverse momentum distributions show an approximately constant value, after a rapid rise at lower energies [3]. These features are not observed in elementary interactions and appear to be unique characteristics of heavy ion collisions. Moreover, these observations have not been reproduced in hadronic transport models or statistical models of hadron production. The data are consistent with the expected signals of the onset of a phase transition in heavy ion collisions at low SPS energies [2, 4]. Recent measurements in Au+Au collisions at the highest available energies at RHIC indicate that in these collisions a highly collective, nearly thermalized system is formed [5], although the nature of the underlying degrees of freedom is still under debate. A comparison of SPS to RHIC data shows a rather smooth evolution of hadronic observables from the higher SPS energies up to the highest RHIC energies [5, 6].

Further information about the existence and nature of a phase transition in the SPS energy range can possibly be gained from studies of event-by-event fluctuations of final state hadron distributions. Several mechanisms have been proposed that could lead to such event-by-event fluctuations, including overheating-supercooling fluctuations due to a first order phase transition with large latent heat [7], and fluctuations due to a phase of coexisting confined and deconfined matter (mixed phase) in varying relative abundances [8]. The presence or absence of such fluctuations might contain otherwise inaccessible information about the nature and order of a phase transition at these energies [9].

Additional motivation for studies of fluctuations in kaon and proton production comes from theoretical studies of the QCD phase diagram [8, 10, 11]. It has been argued that the transition from hadronic to deconfined matter changes from a first order transition at large baryo-chemical potential,  $\mu_B$ , to a second-order transition or a cross-over at small  $\mu_B$ . This implies the existence of a critical endpoint at the end of the first order transition line. If freeze-out of a bulk strongly interacting system occurred close to the critical point, observable non-statistical fluctuations in particle momentum distributions or baryon number correlations could be induced. While theoretical predictions for the location of the critical point and the strength of expected fluctuation signals are still under debate, it is clear that a positive experimental signal for fluctuations related to the critical point could lead to major progress in our understanding of the QCD phase diagram.

To obtain experimental information directly related to the nature of the phase transition from fluctuations, systematic measurements in various regions of the  $\mu_B$  versus temperature  $T$  phase diagram are necessary. The energy density, temperature and baryo-chemical potential probed in the reaction can be controlled by varying the incident energy of the colliding system. This will allow us to test if the observed structure in the energy dependence of event-averaged hadronic signatures is reflected in the collective phenomena probed by event-by-event fluctuations. Preliminary results by NA49 showing a significant energy dependence of fluctuations in the kaon to pion and proton to pion multiplicity ratios were shown in [12]. In this paper, we present final results on the energy dependence of event-by-event fluctuations of these ratios in central Pb+Pb collisions over the SPS energy regime.

Throughout the paper, we will define the event-by-event kaon to pion ratio as  $K/\pi \equiv \frac{N_{K^+} + N_{K^-}}{N_{\pi^+} + N_{\pi^-}}$  and the event-by-event proton to pion ratio as  $(p + \bar{p})/\pi \equiv \frac{N_p + N_{\bar{p}}}{N_{\pi^+} + N_{\pi^-}}$ . Here,  $N_{\pi^\pm}$ ,  $N_{K^\pm}$ ,  $N_p$  and  $N_{\bar{p}}$  denote the observed pion, kaon, proton and anti-proton yields, respectively, within the acceptance for a given event. It is important to note that all multiplicities, particle ratios and fluctuations reported in this paper refer to the observed yields in the experimental acceptance region. For the fluctuation measurement, an extrapolation to full phase space would only be possible using an assumption about the (unknown) nature of the underlying correlations or fluctuations. To allow a detailed comparison of theoretical calculations to the results presented here, 3-dimensional acceptance tables for each collision energy can be provided upon request.

## II. EXPERIMENTAL SETUP AND DATA SELECTION

The data presented here were taken with the NA49 experiment during runs from 1996 to 2002. The NA49 setup is shown schematically in Fig. 1 and described in detail in [13]. Particle trajectories are measured using four large volume Time Projection Chambers (TPCs). Two TPCs, VTPC-1 and VTPC-2, are placed in the magnetic field of two super-conducting dipole magnets. Two other TPCs, MTPC-L and MTPC-R, are positioned downstream of the magnets. The MTPCs were optimized for a high precision measurement of the specific ionization energy loss  $dE/dx$  which provides the main method of particle identification for this analysis. The target, a thin lead foil of about 0.01 interaction length for Pb ions, was positioned 80 cm upstream from VTPC-1.

### A. Event selection

At all five beam energies the most central Pb+Pb collisions were selected based on the energy  $E_{veto}$  deposited

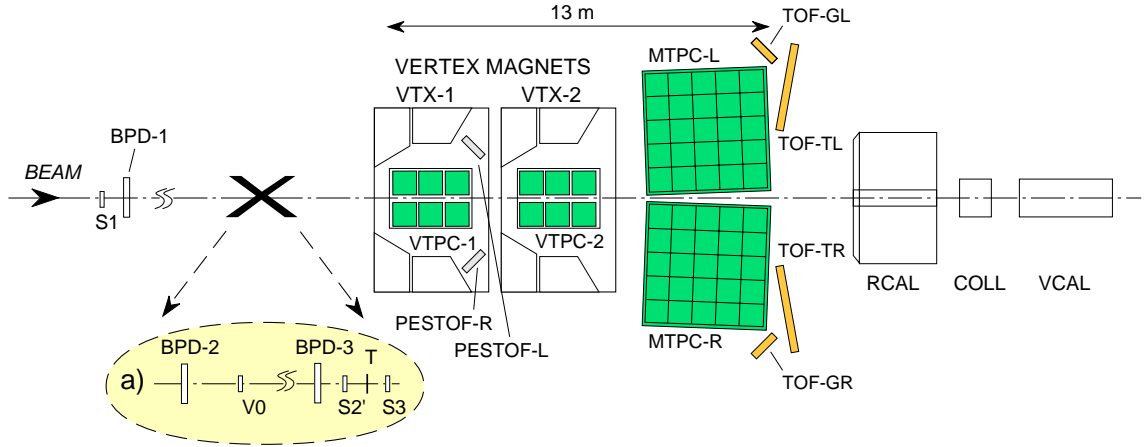


FIG. 1: The experimental set-up of the NA49 experiment [13].

TABLE I: Details of the data sets used in this analysis. For all data sets, the 3.5% most central events were selected.  $y_{CMS}$  is the beam rapidity in the collision center-of-mass frame. The two numbers of tracks/event refer to the strict and loose track quality cuts (see text).

Beam energy (GeV)	$\sqrt{s_{NN}}$ (GeV)	$y_{CMS}$	Year taken	# of events	Tracks/event
20A	6.3	1.88	2002	140k	58 - 66
30A	7.6	2.08	2002	170k	100 - 115
40A	8.7	2.22	1999	160k	141 - 164
80A	12.3	2.56	2000	140k	288 - 347
158A	17.3	2.91	1996	120k	455 - 568

in a downstream calorimeter (VCAL) by projectile spectator nucleons. The geometrical acceptance of the VCAL calorimeter was adjusted for each energy using a collimator (COLL) [13].

Details of the data sets used in this analysis are given in Table 1. We only included the 3.5% most central Pb+Pb collisions at each energy. The tight centrality selection was used to minimize event-by-event fluctuations due to the residual dependence of the kaon to pion ratio on system size and hence centrality. For the selected centrality range, we find that the remaining relative variation of the  $K/\pi$  and  $(p + \bar{p})/\pi$  ratios with  $E_{veto}$  agrees within 1% for the different collision energies, and gives an absolute contribution of less than 1% to the extracted dynamical fluctuation signal. No correction was made for this contribution.

### B. $dE/dx$ particle identification

The overall sensitivity of the  $K/\pi$  fluctuation measurements depends crucially on the resolution and stability of the event-by-event  $dE/dx$  particle identification. To optimize the stability of the  $dE/dx$  measurement with respect to time, variations of event multiplicity and possible background contributions, only the energy loss of the

track in the MTPCs was used in this analysis. The tracking information from VTPC's was used in the momentum determination and for rejecting background from secondary interactions and weak decays.

To eliminate a significant multiplicity dependence of the  $dE/dx$  due to the high charge load on the TPC readout chambers in central Pb+Pb events, a correction algorithm developed specifically for the MTPCs was applied [14]. The response function of the TPC amplifier/shaper was determined by running an iterative shape fitting algorithm over the MTPC data. Using the response function obtained from this procedure, a channel-by-channel correction of the raw TPC charge measurements is performed. This unfolding procedure takes into account the charge history of sets of neighboring channels, which are coupled via crosstalk effects through the sense wires of each TPC readout chamber.

These corrections improve the average  $dE/dx$  resolution by about 30% from  $\sigma_{dE/dx}/\langle dE/dx \rangle = 5-6\%$  to the final value of 3.9% for central Pb+Pb collisions. More importantly, the observed multiplicity dependence of the  $dE/dx$  measurement was reduced by more than 90%, leaving a change of less than 0.3% over the selected multiplicity range. The values are quoted for the highest beam energy, corresponding to the highest multiplicities and charge loads in the TPCs. The performance of the

algorithm was also cross-checked at each beam energy.

The MTPCs detect particles in the forward hemisphere of the collisions. This requires particle identification to be performed in the relativistic rise region, leading to a rather small separation in energy loss between different particle species. To allow for separation of kaons and protons, a cut in total momentum of  $p_{tot} \geq 3$  GeV/c is applied for all data sets. Above this cut, the achieved  $dE/dx$  resolution translates into an average separation of pions from kaons of about  $2.1 \sigma$  and of kaons from protons of about  $1.8 \sigma$ .

In combination with the geometrical acceptance of the TPCs and the track quality cuts, the  $p_{tot}$  cut determines the acceptance function for particles entering the analysis at each beam energy. To minimize the rapidity acceptance shift for kaons, relative to CMS rapidity, the magnetic field settings for the two magnets were changed for each beam energy. Note that in a fixed target setup it is not possible to simultaneously keep the relative rapidity acceptance constant for multiple particles species with different masses. Figure 2 shows the phase space distributions of accepted particles at the different collision energies, assuming pion, kaon and proton mass for the left, center and right columns. For each plot, the solid line indicates the default  $p_{tot} > 3$  GeV/c. The Figure illustrates the shifting acceptance, in particular for pions, in  $(p_T, y)$  due to the changing acceptance and the constant PID cutoff in lab total momentum,  $p_{tot}$ . Shown also are dashed lines for alternative  $p_{tot}$  cuts that were applied to test effects of acceptance variations.

### III. ANALYSIS METHOD

#### A. Event-by-event ratio determination

Due to the finite number of particles detected for single Pb+Pb collisions and the limited particle identification capabilities of a TPC in the relativistic rise region, it becomes crucial to make maximum use of the available information when constructing an estimator for the event-by-event particle ratios. The limited separation between different particle species in the  $dE/dx$  measurement does not permit a simple counting of particles in this experiment. Instead, we use the unbinned distribution of particles in  $(\vec{p}, dE/dx)$  for each event to extract just two parameters,  $K/\pi$  and  $(p + \bar{p})/\pi$  by performing an event-by-event maximum likelihood fit [15, 16].

At each energy, the probability density functions (PDFs) for the particle momenta, normalized to unity,  $F_m(\vec{p})$ , are determined for each particle species ( $m$  = kaons, pions, protons, electrons). We also evaluate the normalized PDFs for the truncated mean energy loss,  $f_m(\vec{p}; dE/dx)$ , as a function of particle momentum for each species.

For the event-by-event fit, the relative yield of different particle species is characterized by parameters  $\Theta_m$ , such that  $\sum_m \Theta_m = 1$ . These parameters are determined for

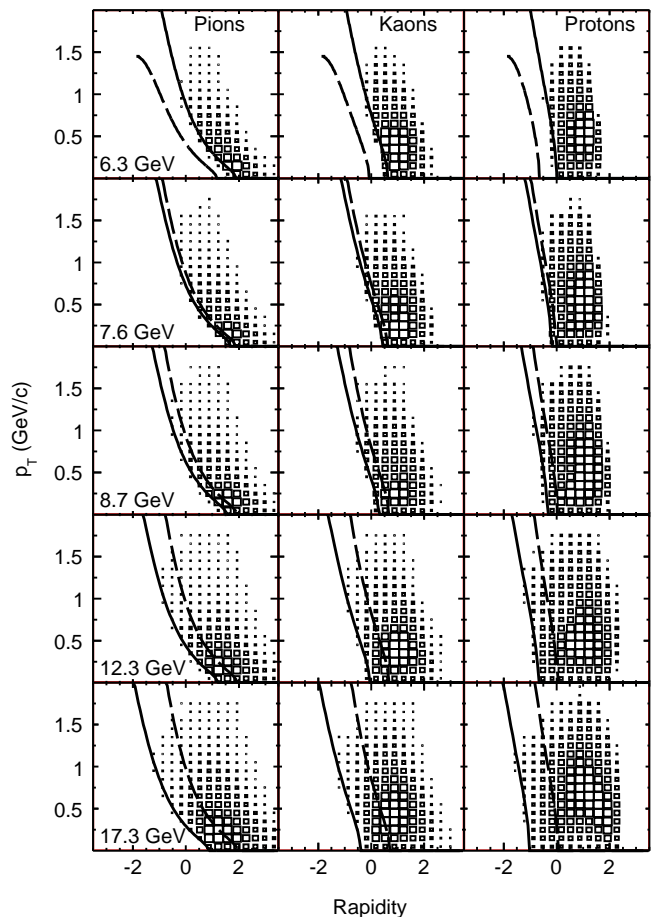


FIG. 2: Phase-space distributions of charged particles used for the fluctuation analysis at all collision energies, from  $\sqrt{s_{NN}} = 6.3$  to 17.3 GeV. Data are shown using pion, kaon and proton mass. The solid line indicates the 3 GeV/c cutoff in total lab momentum. The dashed line indicates cutoffs at each energy that were used for the study of acceptance effects (see text).

each event by maximizing the following likelihood function:

$$L = \prod_{i=1}^n [\sum_m \Theta_m F_m(\vec{p}_i) f_m(\vec{p}_i; (dE/dx)_i)]. \quad (1)$$

Here  $\vec{p}_i$  denotes the observed momentum vector and  $(dE/dx)_i$  the specific energy loss for each particle  $i$  in the event. The parameters  $\Theta_m$  were constrained to be positive for the maximum likelihood fit. The maximum likelihood fit then yields directly the event-by-event  $K/\pi$  and  $(p + \bar{p})/\pi$  particle ratios. No other parameters are fitted event-by-event.

The PDF used in the fit are determined from event-averaged data for each beam energy. The particles from each sample are split into bins in total momentum  $p_{tot}$ , transverse momentum  $p_T$ , azimuthal angle  $\phi$  and charge. The  $dE/dx$  distribution of the particles in each bin is fitted by four Gaussian distributions, one for each particle

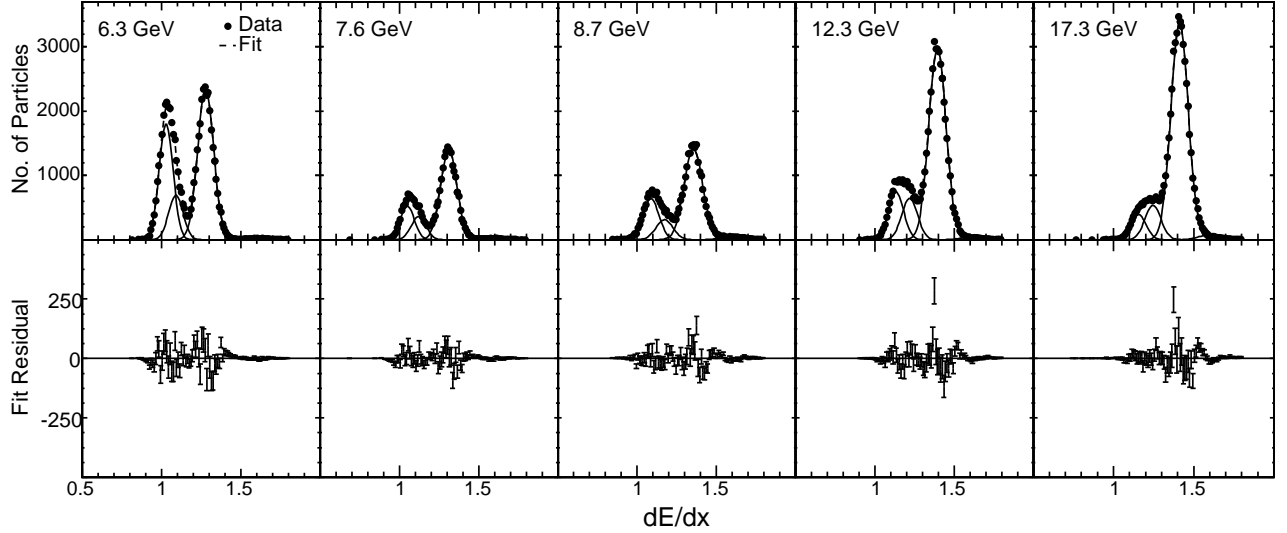


FIG. 3: (Top) Event-averaged  $dE/dx$  distributions (markers) compared to the extracted  $dE/dx$  probability density functions (solid lines) for protons, kaons, pions and the sum of all particles. kaons, pions, protons. For all energies, data distributions and projected PDFs are shown for a narrow momentum range ( $\Delta p_{tot} \approx 1$  GeV/c) for  $200 \text{ MeV/c} < p_T < 400 \text{ MeV/c}$ , close to  $y = 0$  assuming kaon mass. (Bottom) Fit residuals for the sum of  $dE/dx$  probability density functions shown in the upper panels.

species. The fit results for all bins are stored, providing the description of the PDF for each bin. The position and width of the Gaussian distributions describe the  $dE/dx$  PDF,  $f_m$ , while the integrals of the distributions in the momentum bins describe the PDF of the momentum distributions,  $F_m$ .

The top row in Figure 3 shows the event-averaged  $dE/dx$  distributions for positive particles in narrow momentum slices  $\Delta p_{tot} \approx 1$  GeV/c for each of the 5 collision energies. For each energy, the selected region was chosen close to rapidity  $y = 0$ , assuming kaon mass, with transverse momenta  $200 \text{ MeV/c} < p_T < 400 \text{ MeV/c}$ . Also shown in the top row as solid lines are the extracted PDFs for  $p$ ,  $K$ ,  $\pi^+$  and  $e^+$  in the selected momentum slice and the PDF sum. The bottom plots show the residual difference between data and sum PDF, illustrating the quality of the  $dE/dx$  parametrization.

The results of the event-by-event fits for the five data sets are presented in Figure 4, showing the event-by-event ratio distributions for  $K/\pi$  (left) and  $(p + \bar{p})/\pi$  (right). Markers show the  $K/\pi$  and  $(p + \bar{p})/\pi$  distributions for data, while the histogram shows the corresponding reference distributions obtained for mixed events (see below).

## B. Measurement of non-statistical fluctuations

The next step in the analysis is to extract the strength of non-statistical event-by-event fluctuations from the observed distributions of  $K/\pi$  and  $(p + \bar{p})/\pi$ . The relative width  $\sigma$ , defined as  $\sigma = \text{RMS}/\text{Mean} \times 100$  [%], of the

measured event-by-event particle ratio distributions can be decomposed into three contributions:

1. due to the finite number of particles produced and observed per event, the ratio of particle multiplicities measured event-by-event will exhibit statistical fluctuations with a width dictated by the individual particle multiplicities within the acceptance,
2. due to non-ideal particle identification, these statistical fluctuations will be smeared by the experimental  $dE/dx$  resolution and the event-by-event fitting procedure,
3. due to genuine non-statistical fluctuations, which if they exist are superimposed on the background of statistical and experimental fluctuations.

The combined contributions of finite number fluctuations in the particle multiplicities and effects of detector resolution are estimated using a mixed event technique. Mixed events are constructed by randomly selecting measured particles from different events and combining them into artificial events, while reproducing the multiplicity distribution of the real events. By construction, mixed events have on average the same particle ratios as the real events, but no internal correlations. In creating the mixed events, the  $dE/dx$  measurement for each particle is carried over to the mixed events. This allows us to estimate not only the finite-number fluctuations, but also the effect of the finite  $dE/dx$  resolution using mixed events. The mixed events are subjected to the same fit procedure as the real events and the RMS-width  $\sigma_{mix}$  of the mixed

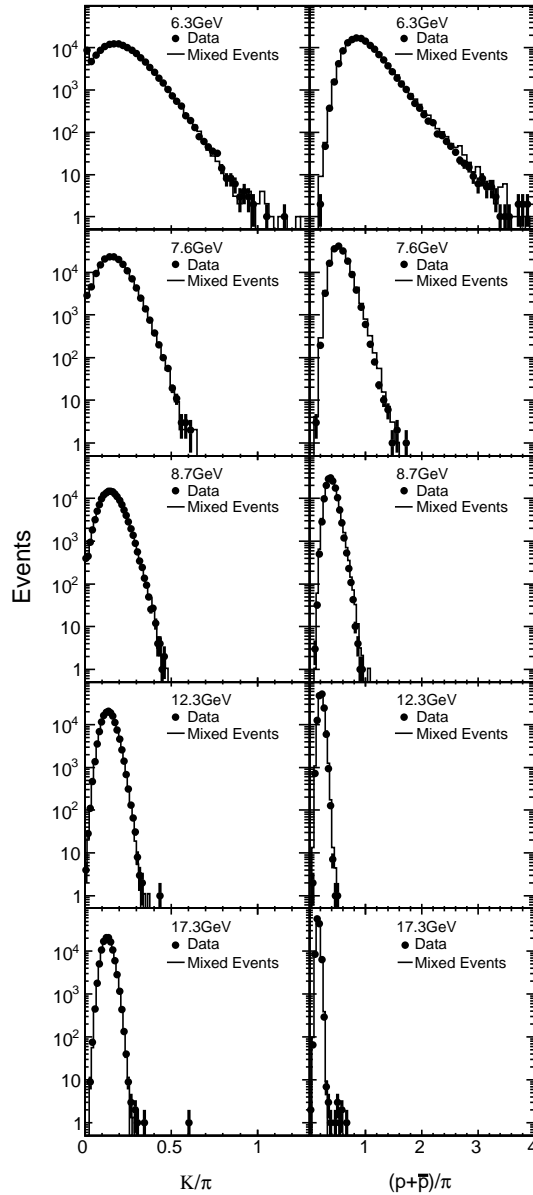


FIG. 4: (Left) Distributions of the event-by-event  $K/\pi$  ratio for data (points) and mixed events (histogram), for all five collision energies. (Right) Distributions of the event-by-event  $(p+\bar{p})/\pi$  ratio for data (points) and mixed events (histogram), for all five collision energies. No acceptance corrections were applied to the particle ratios shown.

event particle ratio distribution is obtained. The results of the event-by-event fit on mixed events are compared in Figure 4 to those from real events. As the figure illustrates, the contributions from the statistical and experimental fluctuations dominate the event-by-event particle ratio distributions, and has to be subtracted carefully.

To extract the physically relevant non-statistical fluctuations from the data distributions as shown in Figure 4, we calculate for each energy the RMS widths of the event-by-event ratio distributions for data and mixed events. The non-statistical fluctuations  $\sigma_{dyn}$  are then es-

timated by subtracting the relative RMS width of data and mixed event distributions in quadrature:

$$\sigma_{dyn} = \text{sign}(\sigma_{data}^2 - \sigma_{mixed}^2) \sqrt{|\sigma_{data}^2 - \sigma_{mixed}^2|} \quad (2)$$

It is important to note that non-statistical fluctuations  $\sigma_{dyn} \neq 0$  can arise from correlated particle production. Possible sources of particle correlations include energy-momentum and quantum-number conservation, quantum correlations and the decay of resonances (which includes strong and electromagnetic decays and a possible contamination due to weak decays). In particular, the definition of  $\sigma_{dyn}$  allows for  $\sigma_{data}^2 < \sigma_{mixed}^2$ , which could result from correlated production of the two particle species forming the ratio, as expected for pion and proton production from hyperon decays.

### C. Systematic uncertainty estimates

As the comparison of the event-by-event particle ratio distributions for data and mixed events shows, the overall width of the distributions is dominated by the fluctuations due to finite particle statistics and resolution. Clearly, the measurement relies on the absence of additional detector-related fluctuations not accounted for by the mixed-event technique and on the reliability of the event-by-event fitting procedure. Several tests on modified mixed events and on input from transport model calculations were performed to verify these requirements. In addition, we varied the event and track selection criteria, as well as the parameters of the  $dE/dx$  fits to estimate the associated systematic uncertainties. The results of these tests are described in the following section. Figures 5–7 show the results for  $K/\pi$  ratios. For all tests, the uncertainties on  $(p+\bar{p})/\pi$  fluctuations were found to be smaller or equal to those on  $K/\pi$  fluctuations. This is expected, as protons are farther separated in  $dE/dx$  from the dominant pion contribution.

#### 1. Linearity of event-by-event fit

Using the PDFs as a function of  $(\vec{p}, dE/dx)$  extracted from the event-averaged data, the particles in the mixed event pool can be assigned a definite mass, such that on average they conform to the known PDFs. This assignment then allows us to create mixed events with the desired multiplicity distribution and adjustable ratios of kaons, pions and protons. Thus we are able to vary both the mean and fluctuations in e.g. the  $K/\pi$  ratio in the mixed events. Using this technique, we created mixed events with  $K/\pi$  ratios varying from 0.08 to 0.26 using the multiplicity distribution for  $\sqrt{s_{NN}} = 17.3$  GeV and subjected these mixed events to the event-by-event fit. As shown in Fig.5, this test demonstrated that over a wide range in  $K/\pi$  the event-by-event ratio estimator is linear with respect to the true  $K/\pi$  ratio in the event.

A small bias of 0.002 in the extracted particle ratio is observed. As the same fitting procedure is used on data and mixed events, this bias will not affect the estimate of  $\sigma_{dyn}$ .

## 2. Sensitivity of fluctuation measurement

The modified mixed events discussed in the previous section also allow us to test the sensitivity of the extraction of non-statistical ratio fluctuations. Using the multiplicity distribution of the 17.3 GeV dataset, non-statistical Gaussian variations of magnitude  $\sigma_{dyn}^{in}$  in the  $K/\pi$  ratio were introduced in the creation of the “signal” mixed events, in addition to the statistical event-by-event variation. For values of  $\sigma_{dyn}^{in}$  from 0 to 20%, the signal mixed events were then run through the full analysis procedure, using unmodified mixed events as the statistical reference. The result of this study is shown in Figure 6, where the extracted fluctuations are compared to the known input amplitude. The extracted magnitude of fluctuations is found to be equal to the input amplitude within statistical errors, even for small input fluctuations of  $\approx 1\%$ . A small systematic uncertainty of 0.2% is assigned to the fitting procedure for both  $K/\pi$  and  $(p + \bar{p})/\pi$  non-statistical fluctuations.

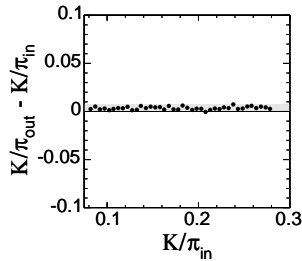


FIG. 5: Difference between measured and input  $K/\pi$  ratio versus average input  $K/\pi$  ratio for mixed events, showing that the event-by-event fit is linear with respect to the input ratio.

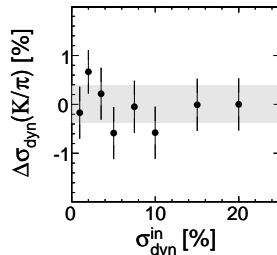


FIG. 6: Relative deviation of extracted  $K/\pi$  non-statistical fluctuations from the input value,  $\sigma_{dyn}^{in}$ , as a function of  $\sigma_{dyn}^{in}$  for modified mixed events (see text). The shaded band indicates the assigned estimate of systematic uncertainty from the fitting procedure as a function of amplitude.

Another concern is the highly non-Gaussian nature of the event-by-event  $K/\pi$  distributions for low particle multiplicities. To check the validity of equation 2 in this case, the observed distributions for mixed events were fitted with Gamma-distributions at each energy. The Gamma-distributions were folded with Gaussians corresponding to the magnitude of non-statistical fluctuations at each energy and sampled to reproduce the input histograms for  $\sigma_{data}^2$ . The unfolded Gamma-distributions

were sampled to obtain  $\sigma_{mixed}^2$ . The resulting  $\sigma_{dyn}$  was plotted for each energy, in comparison to the corresponding input value, in Figure 7(a). This study demonstrates that the magnitude of the Gaussian input fluctuations is recovered from applying equation 2 to the RMS width of the non-Gaussian signal and reference ratio distributions. The effect of low particle multiplicities was also tested by repeating the analysis for the highest energy dataset while randomly removing particles from each event, to resemble the multiplicity distributions in the lower energy datasets. The extracted particle ratios were found to be independent of the fraction of removed particles within statistical errors.

Finally, the analysis method was tested on events simulated with the UrQMD transport code [17]. For these events, non-statistical fluctuations as a function of beam-energy were determined using two methods. The first method determined the event-by-event particle ratios by counting the different particle multiplicities in the NA49 acceptance. The second method assigned a  $dE/dx$  value to each particle according to the  $(\vec{p}, dE/dx)$  PDFs and then performed an event-by-event fit to extract the particle ratios. For each method, the non-statistical fluctuations were extracted by comparison to the respective mixed event reference. As Figure 7(b) demonstrates, the two methods yield the same magnitude of non-statistical fluctuations at each collision energy, within statistical errors. To account for a possible small energy dependence, the systematic uncertainty shown by the shaded area in Figure 7(b) was assigned.

## 3. Fluctuations in the tails of ratio distributions

In Figure 4, several outlier events in the ratio distributions can be seen, in particular for the higher collision energies. To test whether the observed non-statistical fluctuations are due to these outliers or fluctuations in the tails of the ratio distributions, we removed 1% of events with the highest  $K/\pi$  ratio in data and mixed events at each energy. The resulting change of the extracted fluctuation signal is shown by the full symbols in Figure 7(c). Also plotted in this figure is the result of removing the 1% of events with the lowest  $K/\pi$  ratio. As expected, removing either of the tails of the distribution leads to a slight reduction in the extracted dynamical fluctuations  $\sigma_{dyn}$ . In particular for removing the high tail of the distribution, the change is small for most energies. Removing the low end of the distribution has a 10% effect at the low energies. Smaller changes were seen for a corresponding study of  $(p + \bar{p})/\pi$  fluctuations.

As Figure 4 shows, the  $K/\pi$  ratio distributions for the lowest two energies develop a spike at very small  $K/\pi$  ratios. For the  $\sqrt{s_{NN}} = 6.3$  GeV data set, we examined the events in this region for signs of detector or reconstruction failures, but found no anomalies compared to the bulk of events. The spike is also present in the mixed event sample, suggesting that it arises from a combina-

tion of low kaon multiplicities and the finite resolution of the event-by-event maximum likelihood fit. It is important to note that the fit does not allow negative  $K/\pi$  values. To confirm this hypothesis, we studied the ratio of the event-by-event  $K/\pi$  distributions in data and mixed events and found that this ratio does not exhibit a spike at small  $K/\pi$  ratios, but rather shows a smooth increase from the average  $K/\pi$  value of 0.19 down to  $K/\pi \approx 0$ . The shape of this ratio is consistent with the presence of dynamical fluctuations in the data events and with the observed small decrease in  $\sigma_{dyn}$  when removing events in the low tails of the distributions from the analysis.

Finally, we performed further simulations using the UrQMD generator. For generated UrQMD events, event-by-event  $K/\pi$  distributions were obtained by counting particles in the NA49 acceptance and alternatively by assigning energy loss information to each particle and performing the same event-by-event likelihood fit as described before. As expected, a broadening of the event-by-event  $K/\pi$  distribution is seen when using the likelihood fit as compared to particle counting. This leads to an enhanced number of events in the  $K/\pi \approx 0$  bin, reproducing what is seen in the data. However, this enhancement is again well reproduced in the corresponding mixed events and no bias is found compared to an analysis of dynamical fluctuations based on direct counting of particles.

In summary, our studies show that the extreme tails of the distribution do not dominate the overall fluctuation strength. In particular the shape of the  $K/\pi$  distributions for small  $K/\pi$  is well reproduced by the mixed event procedure and in UrQMD studies using simulated energy loss information.

#### 4. Uncertainty in $dE/dx$ scaling

In determining the  $dE/dx$  PDFs, we assume that the width of the  $dE/dx$  distributions for the different particle species scales with the average  $dE/dx$  as  $dE/dx^\alpha$ , with  $\alpha = 0.65$  obtained in previous studies of  $dE/dx$  particle identification [19]. As a function of momentum  $\vec{p}$ , the width for a given particle species also changes due to variations in the observed TPC track length and due to variations in the local track density. In combination with the small separation between different particle species, this makes a precise determination of  $\alpha$  difficult. To test the effect of the uncertainty in  $\alpha$  on the observed fluctuations, we repeated the analysis, starting from the determination of PDFs, for a much larger value of  $\alpha = 1.15$ . The difference between the fluctuation results obtained for  $\alpha = 1.15$  and  $\alpha = 0.65$  is shown in Figure 7(d). The fluctuations are seen to be rather robust against changes in  $\alpha$ , with the difference only reaching up to 1% for the lower collision energies. Even smaller variations are seen in the  $(p + \bar{p})/\pi$  fluctuations. The actual uncertainty in  $\alpha$  is estimated to be only  $\pm 0.15$ , leading to the systematic uncertainty estimate shown as the shaded band in

Figure 7(d).

#### 5. Track quality cuts

In order to test for possible systematic distortions of the fluctuation measurement not included in the MC simulations, we used two sets of quality cuts in the event and track selection for the analysis. The corresponding datasets should have different sensitivity to detector and tracking effects, such as contributions from weak decays and secondary interactions, or effects from varying track densities on reconstruction and particle identification. The quality cuts are based on the distance of closest approach of the extrapolated particle trajectory to the main vertex, the length over which the track was measured in the TPC and the number of measured points on the track. For the set of loose quality cuts, the cuts on the extrapolation of tracks to the primary vertex and a cut on the track fit quality were removed. As shown in Table 1, the difference in multiplicity for the two samples varies with increasing track density and changing acceptance, as the collision energy increases, and ranges from 10% at the lowest energy to about 20% at the highest energy. The track selection using loose track quality cuts yields more tracks per event to include in the event-by-event particle ratio estimation, but possibly also increases the contamination of the track sample with non-primary and background particles.

The final value of the fluctuation signal presented below is calculated as the arithmetic mean of the results from both samples. Figure 7(e) shows the deviation from the average result for the tight track-cut sample. The shaded area indicates the estimated systematic uncertainty in the final result for  $K/\pi$  fluctuations related to the track selection. The same study was performed for  $(p + \bar{p})/\pi$  fluctuations, resulting in a smaller variation than seen for  $K/\pi$ . The corresponding contribution to the systematic uncertainty on the  $(p + \bar{p})/\pi$  non-statistical fluctuations is shown by the dashed lines in Figure 7(e).

#### 6. Effects of acceptance variation

As discussed above, the constant PID cutoff in lab total momentum  $p_{tot} > 3$  GeV/c, below which particles species cannot reliably be separated, leads to a significantly changing acceptance at different beam energies (see Fig. 2). To study the influence of the changing acceptance relative to the lowest beam energy, we modified the cutoff for the four higher beam energies to 3.6, 4.4, 6.3 and 9.1 GeV/c, respectively. These higher cutoffs remove low  $p_T$  particles near midrapidity approximating the default cutoff for the  $\sqrt{s_{NN}} = 6.3$  GeV data sample. The resulting change in the  $K/\pi$  fluctuation signal is plotted as the filled symbols in Figure 7(f), showing a rather small difference compared to the standard



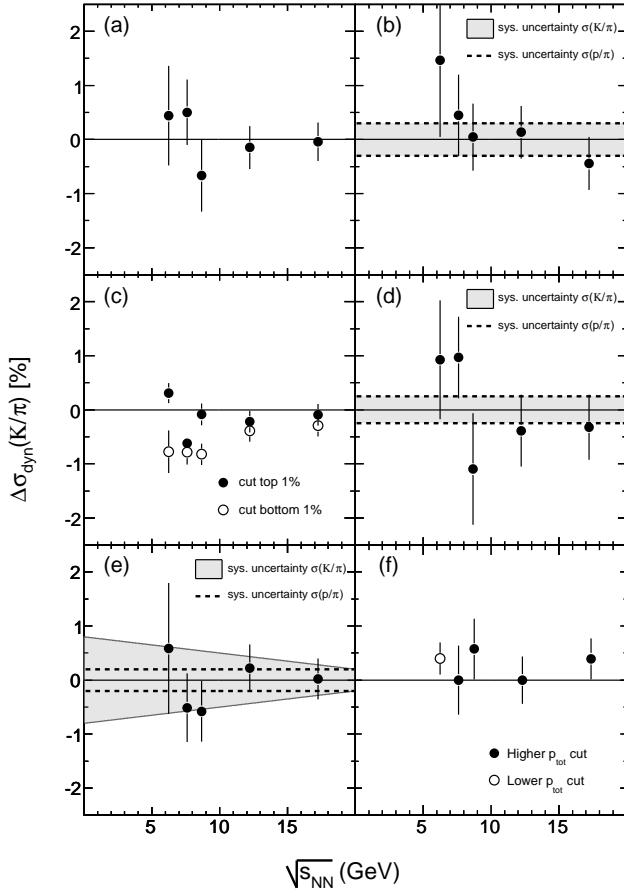


FIG. 7: Results of various studies on systematic uncertainties in the determination of  $\sigma_{dyn}(K/\pi)$ : (a) extraction of  $\sigma_{dyn}$  using equation 2. (b)  $dE/dx$  fit versus particle counting in UrQMD. (c) removal of tails of event-by-event distributions. (d) variation of  $dE/dx$  width scaling. (e) variation of track quality cuts. (f) variation of  $p_{tot}$  cutoff. Shaded bands indicate the contribution to the systematic error for  $K/\pi$  fluctuations. Where applicable, dashed lines indicate corresponding contribution to systematic error for  $(p + \bar{p})/\pi$  fluctuations. See text for details.

acceptance cut. We also studied a reduced  $p_{tot}$  cut of 1.45 GeV/c for the lowest energy data set. The region  $1.45 \text{ GeV/c} < p_{tot} < 3 \text{ GeV/c}$  yields little separation between kaons and protons, but extends the pion acceptance closer to mid-rapidity. The corresponding fluctuation signal is shown as the open symbol in Figure 7(f). Again, no strong change in the  $K/\pi$  non-statistical fluctuations is observed. Note that the event multiplicity is changed by up to 30% by the modified cuts, such that part of the change observed is likely due to statistical fluctuations. As any remaining variation could be due to the physical nature of the non-statistical fluctuations, no systematic uncertainty is assigned for the acceptance variations.

While this study indicated that the results for  $K/\pi$

fluctuations only have a moderate dependence on the details of the acceptance, we need to stress again that a detailed comparison to theoretical models needs to take the experimental acceptance into account. As the measurement is performed within a limited acceptance, particle ratio fluctuations within the acceptance can in principle be caused by non-statistical variations of e.g. the kaon phase space distribution, rather than a non-statistical variation of the  $K/\pi$  ratio in full phase space. Note however that purely statistical variations of the phase-space distributions are removed by comparison to the mixed event reference.

#### IV. RESULTS AND DISCUSSION

The event-by-event  $K/\pi$  and  $(p + \bar{p})/\pi$  ratios shown in Figure 4 exhibit smooth distributions at all five collision energies and show no evidence for the existence of distinct event classes. Qualitatively the  $K/\pi$  ratio distributions are found to be wider than the statistical reference for all energies, while the  $(p + \bar{p})/\pi$  ratio distributions are narrower than the respective reference.

The deviation from the statistical reference  $\sigma_{dyn}$ , as defined in equation 2, is plotted in Figure 8 for  $K/\pi$  fluctuations (top) and  $(p + \bar{p})/\pi$  fluctuations (bottom). The observed non-statistical fluctuations of the  $K/\pi$  ratio are positive and decrease with collision energy. For the highest collision energy, a value of  $\sigma_{dyn} = 3.2 \pm 0.4(\text{stat.}) \pm 0.5(\text{syst.})\%$  is observed, in agreement with the results reported in [15] for an independent dataset. Towards lower collision energies, a steep increase of the fluctuation signal is observed, the  $K/\pi$  fluctuations reaching a value of  $\sigma_{dyn} = 7.9 \pm 1.2(\text{stat.}) \pm 1.0(\text{syst.})\%$  for the lowest energy. The increase is qualitatively consistent with calculations assuming the presence of a deconfinement phase transition at the lowest collision energies of the CERN SPS [18]. This scenario predicts small and energy-independent fluctuations in the  $K/\pi$  ratio in the QGP phase, while for the confined phase large fluctuations are expected that increase towards lower collision energies.

For the  $(p + \bar{p})/\pi$  ratio, which has not been previously reported, the non-statistical fluctuation measure  $\sigma_{dyn}$  is negative for all collision energies. For the lowest collision energy a value of  $\sigma_{dyn} = -8.1 \pm 0.4(\text{stat.}) \pm 1.0(\text{syst.})\%$  is observed. The negative value of  $\sigma_{dyn}$  for  $(p + \bar{p})/\pi$  fluctuations reflects the fact that the width of the data distribution is smaller than the width of the distribution of mixed events for this ratio. A negative fluctuation signal of the event-by-event  $(p + \bar{p})/\pi$  ratio can result from resonance decays into pions and protons. Such contributions correlate the pion and proton multiplicities event-by-event, and thus lead to smaller fluctuations in the ratio than expected from independent particle production. The magnitude of the negative fluctuation signal in the  $(p + \bar{p})/\pi$  channel is then related to the relative contribution of resonance decay products in the final state of the collision.

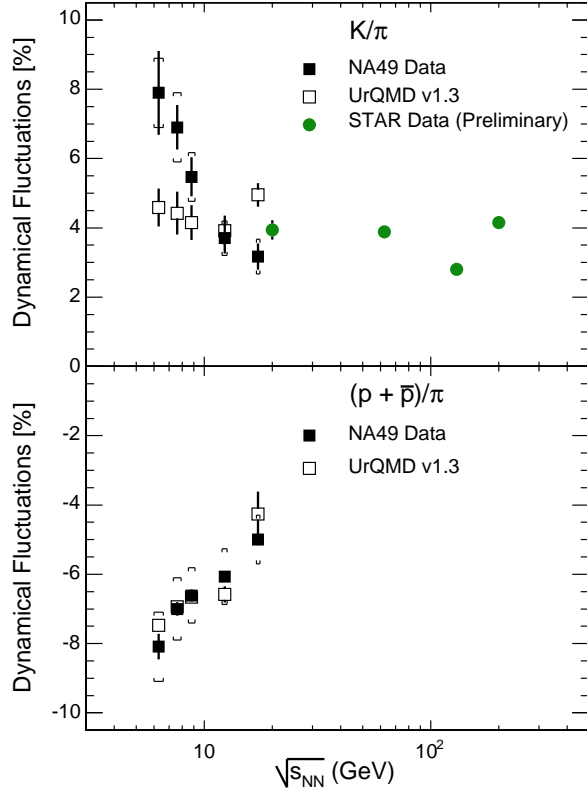


FIG. 8: Energy dependence of the event-by-event non-statistical fluctuations of the  $K/\pi$  ratio (top panel) and the  $(p + \bar{p})/\pi$  ratio (bottom panel). Filled symbols show data, open symbols show calculations with the UrQMD transport code, using NA49 acceptance tables. Systematic uncertainties are shown as brackets.

In order to further estimate the influence of known correlations in the events, like those induced by conservation laws and particle production from resonance decays, we analyzed fluctuations of the  $K/\pi$  and  $(p + \bar{p})/\pi$  ratios in a string-hadronic cascade model, UrQMD [17]. In this model, by construction, no fluctuations due to a potential phase transition are present. For this study, large samples of UrQMD events were generated at all five collision energies and then subjected to an acceptance filter modeling the NA49 detector system. The accepted final state particles were counted and the corresponding ratios were formed for each event. The energy dependence of the event-by-event  $(p + \bar{p})/\pi$  ratio fluctuations in UrQMD closely matches the energy dependence observed in the data, as shown in the bottom plot in Figure 8. This lends further support to interpreting the negative fluctuation signal as resulting from resonance decays, which are the dominant source of  $(p + \bar{p})/\pi$  fluctuations in UrQMD.

The energy dependence of the  $K/\pi$  ratio fluctuation signal however is not reproduced in the cascade model, which gives an energy independent fluctuation signal.

Further studies are needed to determine whether the finite non-statistical  $K/\pi$  fluctuations in UrQMD originate from resonance decays or correlated particle production due to conservation laws.

The  $K/\pi$  fluctuation signal in the data taken at  $\sqrt{s_{NN}} = 17.3$  GeV collision energy was found to be consistent with calculations performed assuming a grand canonical ensemble without enforcing local conservation laws [20]. The small fluctuations at this energy are thus consistent with every event being a random sample from the identical thermal ensemble. The interpretation of the observed increase of  $K/\pi$  fluctuations towards lower energies is complicated by the simultaneous decrease in true particle multiplicities towards lower energies. Stephanov has pointed out that the observed energy dependence could approximately be understood as the combination of a fixed pair-wise correlation strength, in combination with the known dependence of the average event multiplicity on collision energy [21]. Within the experimental resolution of the present measurement alone, the multiplicity scaling expected from this argument can not be ruled out.

Recently, the STAR collaboration has reported preliminary results for non-statistical  $K/\pi$  fluctuations in central Au+Au collisions in the RHIC energy range from  $\sqrt{s_{NN}} = 19.6$  to 200 GeV [22]. The reported results for 19.6 GeV are in agreement with the values quoted here for  $\sqrt{s_{NN}} = 17.3$  GeV, within statistical errors. Although a detailed quantitative comparison of the results suffers from the differences in the NA49 and STAR acceptances, it is important to note that the STAR data show no significant energy dependence, in contrast to the results reported here for the SPS energy range. If confirmed, this would rule out, or at least limit the range of validity, for the proposed multiplicity scaling discussed above.

## V. SUMMARY

We have presented a study of the energy dependence of non-statistical event-by-event fluctuations of the  $K/\pi$  and  $(p + \bar{p})/\pi$  ratios in the energy range  $6.3 < \sqrt{s_{NN}} < 17.3$  GeV. A strong increase of the  $K/\pi$  fluctuation signal is observed towards the low end of this energy range. The increase of the signal is not reproduced by the UrQMD hadronic cascade model, suggesting the onset of a new source of fluctuations. The same model is however able to describe the strong fluctuations seen in the  $(p + \bar{p})/\pi$  ratio. The domain of increased  $K/\pi$  fluctuations coincides with the energy range where a change in the behavior of event-averaged hadronic observables in heavy-ion collisions occurs, relative to elementary collisions. Further theoretical calculations will be needed to evaluate the relevance of this observation for a possible interpretation in the context of a deconfinement phase transition.

This work was supported by the US Department of Energy Grant DE-FG03-97ER41020/A000, the Bundesministerium für Bildung und Forschung, Germany, the Polish

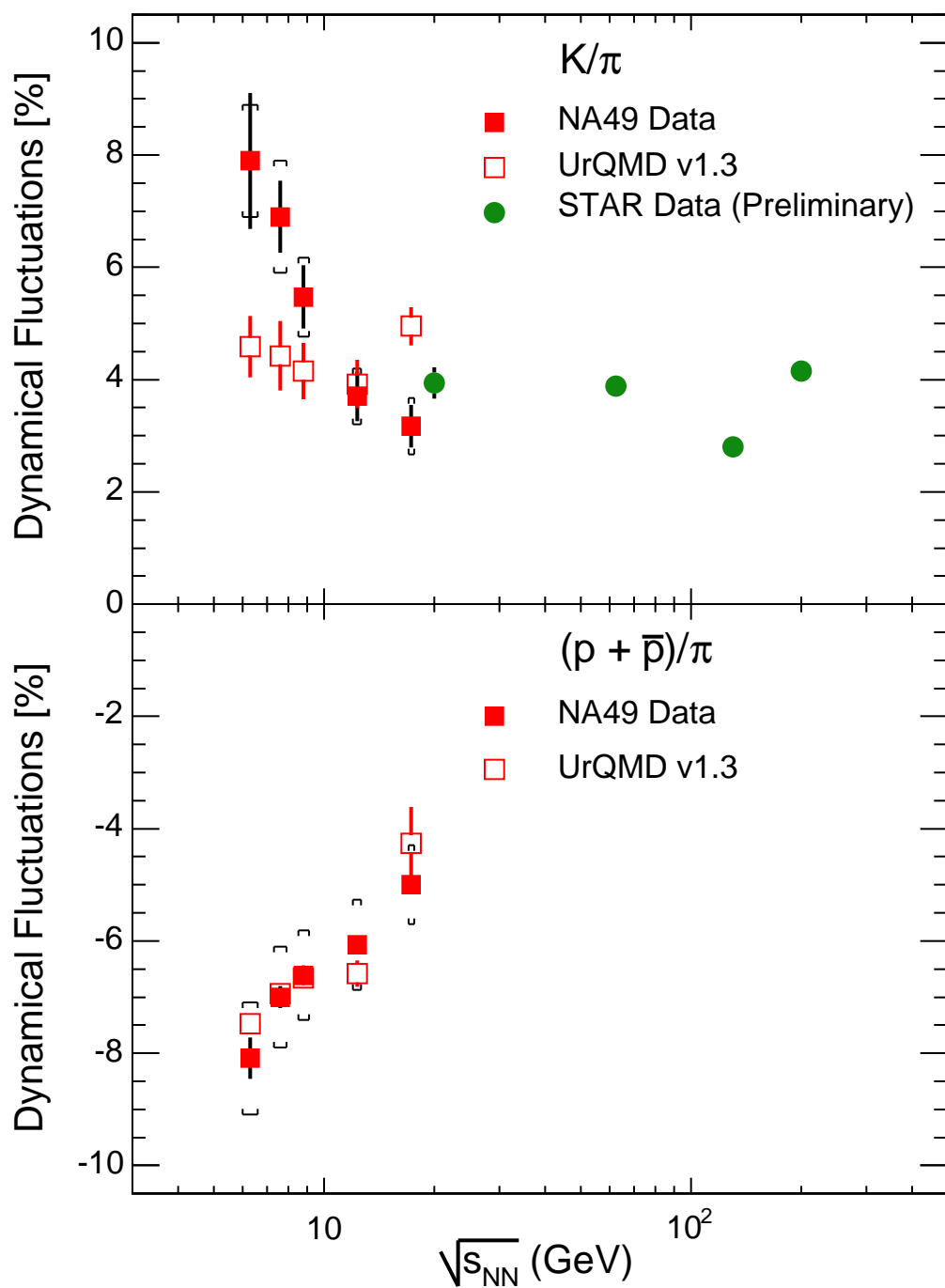
State Committee for Scientific Research (1 P03B 006 30, 1 P03B 097 29, 1 P03B 121 29, SPB/CERN/P-03/Dz 446/2002-2004, 2 P03B 04123), the Hungarian Scientific Research Foundation (T032648, T032293, T043514),

the Hungarian National Science Foundation, OTKA, (F034707), the Polish-German Foundation, and the Korea Science & Engineering Foundation Grant (R01-2005-000-10334-0)

- 
- [1] For an early review, see e.g. E. V. Shuryak, Phys. Rept. **61**, 71 (1980).
  - [2] C. Alt *et al.*, Phys. Rev. **C77**, 024903 (2008).
  - [3] M. Gazdzicki *et al.* [NA49 Collaboration], J. Phys. G **30**, S701 (2004)
  - [4] M. Gaździcki and M. I. Gorenstein, Acta Phys. Polon. **B30**, 2705 (1999) and references therein.
  - [5] I. Arsene *et al.*, Nucl. Phys. A **757**, 1 (2005),  
K. Adcox *et al.*, Nucl. Phys. A **757**, 184 (2005),  
B. B. Back *et al.*, Nucl. Phys. A **757**, 28 (2005),  
J. Adams *et al.*, Nucl. Phys. A **757**, 102 (2005).
  - [6] B. Alver *et al.*, Phys. Rev. Lett. **96**, 212301 (2006).
  - [7] L. P. Csernai and I. N. Mishustin, Phys. Rev. Lett. **74**, 5005 (1995).
  - [8] J. I. Kapusta and A. Mekjian, Phys. Rev. **D33** 1304 (1986).
  - [9] R. Stock, Nature **337** 319 (1989).
  - [10] M. Gazdzicki, M. I. Gorenstein and St. Mrowczynski, Phys. Lett. **B585**, 115 (2004).
  - [11] M. A. Stephanov, K. Rajagopal and E. V. Shuryak, Phys. Rev. Lett. **81**, 4816 (1998),  
for a review, see M. Stephanov, Prog. Theor. Phys. Suppl. **153**, 139 (2004).
  - [12] C. Roland *et al.* [NA49 Collaboration], J. Phys. G **30**, S1381 (2004).
  - [13] S. V. Afanasiev *et al.*, Nucl. Inst. Meth. **A430**, 210 (1999).
  - [14] C. Roland, PhD Thesis, Universität Frankfurt (1999) (available at <https://edms.cern.ch/file/816020/1>).
  - [15] S. V. Afanasiev *et al.*, Phys. Rev. Lett. **86**, 1965 (2001).
  - [16] M. Gazdzicki, Nucl. Instr. and Meth. **A345**, 148 (1994).
  - [17] We used UrQMD version 1.3. See M. Bleicher *et al.*, J. Phys. **G25** 1859 (1999).
  - [18] M. I. Gorenstein, M. Gazdzicki and O. S. Zozulya, Phys. Lett. B **585**, 237 (2004).
  - [19] M. van Leeuwen, PhD Thesis, Universiteit Utrecht (2003) (available at <https://edms.cern.ch/file/816033/1>).
  - [20] S. Jeon and V. Koch, Phys. Rev. Lett. **83**, 5435 (1999).
  - [21] M. Stephanov, private communication.
  - [22] S. Das [STAR Collaboration], J. Phys. **G32** S541, Proceedings of “Strangeness in Quark Matter 2006”.

This figure "Fig8\_20080809.gif" is available in "gif" format from:

<http://arxiv.org/ps/0808.1237v2>



This figure "Fig8\_20080809\_color.gif" is available in "gif" format from:

<http://arxiv.org/ps/0808.1237v2>